ARMA 19–1826

Geomechanical Characterization of a Granodiorite Rock Specimen from Patua Geothermal Field

KC, B., Foroutan, M., Kamali-Asl, A., and Ghazanfari, E.
University of Vermont, Burlington, VT, USA
Cladouhos, T.T.
Cyrq Energy Inc., Seattle, WA, USA

ABSTRACT: Geo-mechanical properties of geothermal reservoir rocks are important in different stages of geothermal resources development, including drilling optimization, reservoir stimulation (or re-stimulation) and development of fluid-flow and multi-physical (thermo-hydro-chemo-mechanical) constitutive models. Laboratory experiments were performed on a cylindrical granodiorite rock specimen retrieved from a well at a depth of 5561.5 ft in Patua geothermal field in Northern Nevada. In this study, Autolab 1500 (a high-pressure/temperature fully servo-controlled triaxial instrument) was used to perform a cyclic and triaxial multi-stage elastic tests on the granodiorite specimen in order to characterize the hysteresis, elastic-plastic, and strength properties of the specimen under different loading conditions. Laboratory results revealed linear elastic with very small (or no) plastic deformation and pressure dependent mechanical responses of the specimen under stresses up to 50 MPa of confining and 60 MPa of differential stress. Young's modulus and Poisson's ratio of the specimen under different stress conditions are reported in the paper. Within the elastic region, the Young's modulus increased, while the Poisson's ratio decreased with the increment of the differential stress during loading stage. Moreover, the effect of the closure of the micro-cracks present in the specimen was observed in specimen's response at lower stress levels.

1. INTRODUCTION

Geothermal energy is considered as a sustainable source of energy and has the capacity of producing up to 100 GW of electricity in the United States by 2050 (Tester et al., 2006). A geothermal system involves injecting cold fluid and extracting the heated fluid from the deep reservoirs, often time crystalline rock formations such as granodiorite (e.g. Tester et al., 2006; Guo et al., 2011). One of the most well-known barriers to the development of geothermal systems is production decline, which is often due to permeability deficiency and poor fracture network connectivity (e.g. Ghassemi, 2012; Kamali-Asl et al., 2018a; White et al., 2018). To overcome this problem, often times hydro-shearing (e.g. Riahi and Damjanac, 2013; Cladouhos et al., 2016), hydraulic fracturing (e.g. Oldenburg et al., 2016; Watanabe et al., 2017), or mixed stimulation (e.g. McClure and Horne, 2014) is implemented to enhance the permeability by increasing the fracture network connectivity, and hence, increase the productivity of an Enhanced Geothermal System (EGS).

Granodiorites, classified as intrusive igneous rock, are often found in white-to-light grey color (e.g. Sarjoughian and Kananian, 2017; Pour et al., 2018). The mineral composition of granodiorite is similar to both granite and diorite. However, it contains higher amount of mafic minerals compared to granite and more quartz content compared to diorite (Glazner et al., 2018). The most abundant minerals of the granodiorite rocks are K-feldspars, plagioclase feldspars, and quartz (Kumar et al., 2017). The granodiorite rocks are widely encountered in geothermal formations (e.g. Zhang et al., 2018). Studies suggest that the mechanical properties of the granodiorite rocks are affected by the presence of micro-cracks, foliation, and anisotropy (e.g. Nejati, 2018) and fluctuation of stress and temperature condition in field (e.g. Kwon et al., 2018; Zhang et al., 2018).

The Patua geothermal field operated by Gradient Resource Inc. includes 13 hot springs ranging in temperature from 82 to 394 °F. The site is located at the southern end of the Hot Springs Mountains in Lyon and Churchill counties near Hazen, Nevada (Garc et al., 2015). The reservoir lies at Walker Lane-Great Basin

tectonic settings, where the NW striking intersects with NE striking basin (Combs et al., 2012). The geological structure of the reservoir involves multiple layers of volcanic rocks underlain primarily by fractured granitic rocks (Peterson et al., 2011). Moreover, results from the exploration program composed of geological, geochemical, and geo-mechanical investigations coupled with 30 days of injection test proved the poor fracture connectivity among the granitic layers of the reservoir (Combs et al., 2012).

Since the mechanical behavior of the rocks are influenced by alteration in reservoir conditions (i.e. pressures and temperature), estimation of the geo-mechanical properties of geothermal rocks (e.g. elastic moduli, strength and failure properties) is of crucial importance. These parameters serve as critical input parameters for numerical models that aim to predict the rock response under different pressure and temperature conditions (e.g. Motra and Stutz, 2018). Furthermore, the crystalline rock formations (e.g. granite and granodiorite) usually exhibit very low (i) matrix permeability, and (ii) pore connectivity to extract the injected fluid. Therefore, hydraulic stimulation techniques are usually considered to re-open the existing sealed fractures or creating a new fracture network inside the reservoir (e.g. McClure and Horne, 2014; Cladouhos et al., 2016; Oldenburg et al., 2016). Hydraulic stimulation programs usually involve alteration of the stress regime and activation of pre-existing faults and discontinuities in the reservoir. Hence, knowing the strength properties and failure behavior of the geothermal rock is crucial in order to perform a safe and optimized reservoir stimulation plan (e.g. Lutz et al., 2010; Weiner et al., 2019).

The main purpose of this study is to evaluate the variation of elastic properties (e.g. Young's, shear, and bulk moduli, and Poisson's ratio) of the granodiorite rock specimen under various stress conditions. In order to investigate the pressure dependency of the elastic properties, gradual degradation of elasticity, and hysteresis behavior, multi-stage elastic and cyclic tests were performed on the specimen.

2. MATERIALS

The granodiorite specimen used in the study was retrieved from well 35-16 at a depth of 5561.5 ft located in Patua geothermal field. The original core as obtained from the well had a diameter of 1.9 and a length of 6 inches, dry density of 2.68 g/cm^3, and porosity of approximately 0.7%. Two inclined natural fractures were present in the original core. X-Ray Diffraction (XRD) analysis revealed that the rock was composed of 68% albite, 31.8% quartz, 0.2% biotite and traces of chlorite.

3. EXPERIMENTAL METHODOLOGY

3.1. Sample Preparation

Rock specimen was prepared following ASTM D4543 Standard. The original core (see Fig. 1(a)) was saw cut and the two ends were lapped to 0.001 inches to obtain an intact specimen with a diameter of 48 mm and a length of 41 mm (Fig. 1(b)). Although it was desired to prepare a specimen with aspect ratio greater than 2, the existing fractures in the received core (see Fig. 1(a)) constrained preparing a specimen with such aspect ratio. Higher compressive strength of the rock specimen was observed for smaller aspect ratio (e.g. Pellegrino et al., 1997; Yan et al., 2017; Wang et al., 2018). However, Young's modulus of the specimen (granite) remained relatively unaffected by the aspect ratio (e.g. Li et al., 2005). A copper jacket was wrapped around the specimen to facilitate attachment of the strain gauges and prevent leakage of confining fluid into the specimen. Since the copper jacket wrapped around the specimen was very thin (38 gauge i.e. ~ 0.15 mm thickness) and was sitting perfectly on the rock surface, the deformations measured by the strain gauges are true deformations of the specimen. Two core-holders were wire-tightened to the two ends of the specimen using Viton jacket (Fig. 1(c)). The interface between the Viton and copper jackets was sealed using high temperature/pressure resistant epoxy as an extra precaution to avoid leakage of the confining fluid (Fig. 1(c)). Then, a set of axial and radial strain gauge was attached on the copper jacket, and the specimen was placed inside the test vessel (Fig. 1(d)). X-Ray CT image of the specimen (Fig. 1(e) and (f)) revealed the presence of the micro-cracks in the specimen.

3.2. Experimental Procedure

Mechanical tests on the specimen were performed using Autolab 1500, which is a high pressure/temperature fully servo-controlled triaxial equipment. Deformation of the rock specimen, measured by the axial and radial self-temperature-compensated strain gauges, was used to estimate the elastic moduli of the specimen.

3.2.1. Estimation of Static Moduli

A material is considered to obey the rules of Vertical Transverse Isotropic (VTI) medium, if its characteristics are symmetric about an axis normal to the plane of isotropy (e.g. Puzrin, 2012, Villamor Lora et al., 2016; Kamali-Asl et al., 2019a). Like many other rock specimens, granodiorite can be modelled as a VTI medium with vertical symmetry axis. In a triaxial setup with a vertical axis as an axis of symmetry, the compliance matrix can be written as (e.g. Villamor Lora et al. 2016; Kamali-Asl et al, 2019a):

$$\begin{Bmatrix} \delta\varepsilon_a \\ \delta\varepsilon_r \end{Bmatrix} = \begin{bmatrix} \frac{1}{E_v} & -\frac{2\nu_{vh}}{E_v} \\ -\frac{2\nu_{vh}}{E_v} & -\frac{(1-\nu_{hh})}{E_h} \end{bmatrix} \times \begin{Bmatrix} \delta\sigma_a \\ \delta\sigma_r \end{Bmatrix} \qquad (1)$$

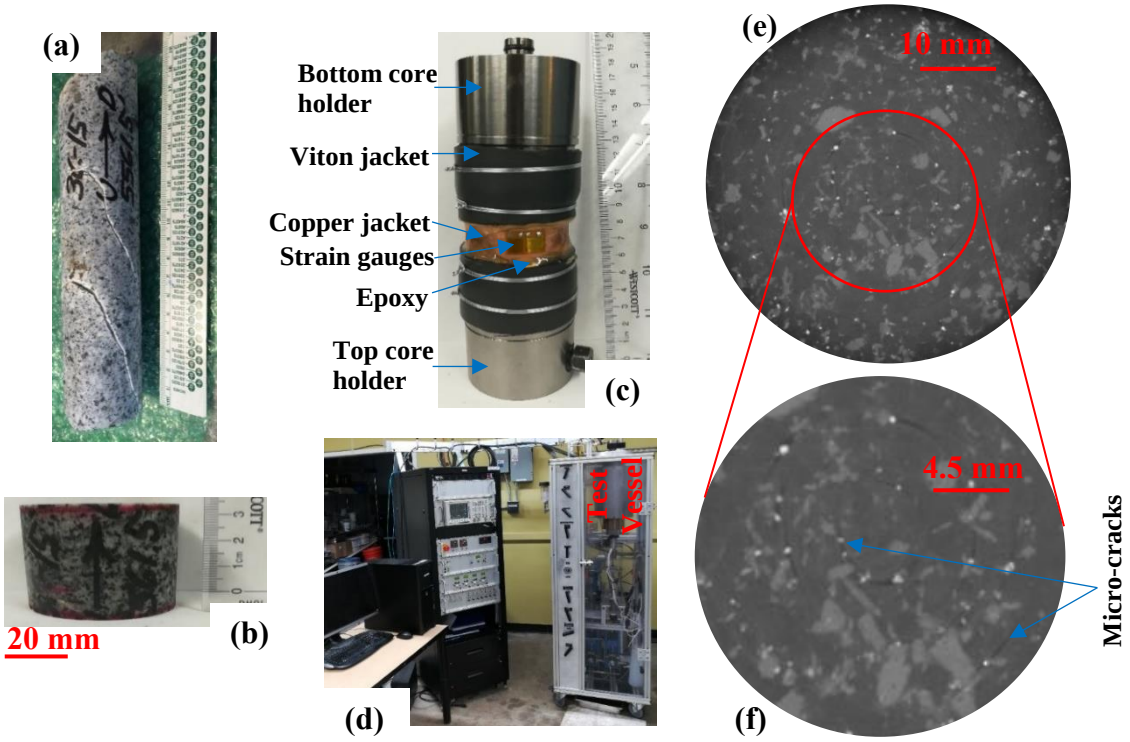

Fig. 1. Photo of (a) original core retrieved from the well, (b) intact granodiorite specimen, (c) specimen wire-tightened to the core-holders, (d) Autolab 1500 instrument, (e) X-Ray CT image of a cross-section of the specimen, and (f) Zoomed section of the CT image showing the micro-cracks present in the specimen

where E_h and E_v represent Young's moduli in horizontal and vertical directions, respectively. ν_{hh} and ν_{vh} are the Poisson's ratios in the horizontal direction caused by horizontal and vertical compressions, respectively. ε_a and ε_r are strain on axial (i.e. vertical) and radial (i.e. horizontal) directions, respectively. σ_a and σ_r are stresses on vertical and horizontal directions, respectively.

Eq. (1) can be modified using the definitions of the triaxial strain increment and stress quantities as shown in Eq. (2) (e.g. Puzrin, 2012; Villamor Lora et al., 2016; Kamali-Asl et al., 2019a):

$$\begin{Bmatrix} \delta\varepsilon_v \\ \delta\varepsilon_s \end{Bmatrix} = \begin{bmatrix} \frac{1}{K} & -\frac{1}{J} \\ -\frac{1}{J} & -\frac{1}{3G} \end{bmatrix} \times \begin{Bmatrix} \delta p \\ \delta q \end{Bmatrix} \quad (2)$$

where K is the bulk modulus during isotropic compression (i.e. $\delta q = 0$), J is the coupling modulus, G is the shear modulus for pure shear (i.e. $\delta p = 0$). Mean stress (p), differential stress (q), volumetric strain (ε_v), and distortional strain (ε_s) can be calculated using following equations:

$$\varepsilon_v = \varepsilon_a + 2\varepsilon_r \quad (3)$$

$$\varepsilon_s = \frac{2}{3}(\varepsilon_a + 2\varepsilon_r) \quad (4)$$

$$p = \frac{1}{3}(\sigma_a + 2\sigma_r) \quad (5)$$

$$q = (\sigma_a - \sigma_r) \quad (6)$$

Stress-strain data from the isotropic compression stage of the triaxial experiment was used to determine the bulk modulus (K) and coupling modulus (J) as shown in Fig. 2(a) and (b), respectively. Shear modulus (G), Young's modulus (E), and Poisson's ratio (ν) were estimated using stress-strain response from triaxial stage, as illustrated in Fig. 2(c), (d), and (e), respectively. Estimation of K and J in the last stage of isotropic compression is illustrated in Fig. 2(a) and (b), and estimation of E, ν and G using the average slope of linear portion of the stress-strain response is shown in Fig. 2(c) , (d) and (e).

3.3. Experimental Program

In this study, Multi-Stage Elastic (MSE) and cyclic tests were performed on the dry specimen to characterize the hysteresis and elasto-plastic behavior of the specimen under various loading cycles. During these tests, the stress-strain data were collected to estimate the static moduli at different stress levels. In both MSE and cyclic tests, the rate of load application was maintained at 0.333 MPa/sec for confining pressure (CP) and differential stress (DS) (ASTM D7012). The details of the tests are discussed in following sections.

3.3.1. Multi-Stage Elastic (MSE) Triaxial Test

Due to sample scarcity and variability, multi-stage triaxial tests are usually helpful as a substitute to multiple single-stage triaxial tests (e.g. Villamor Lora et al., 2016; Kamali-Asl et al., 2018b, 2019a). Pressure-dependent elastic, and non-linear properties of a rock specimen can be investigated through MSE tests (e.g. Islam and Skalle,

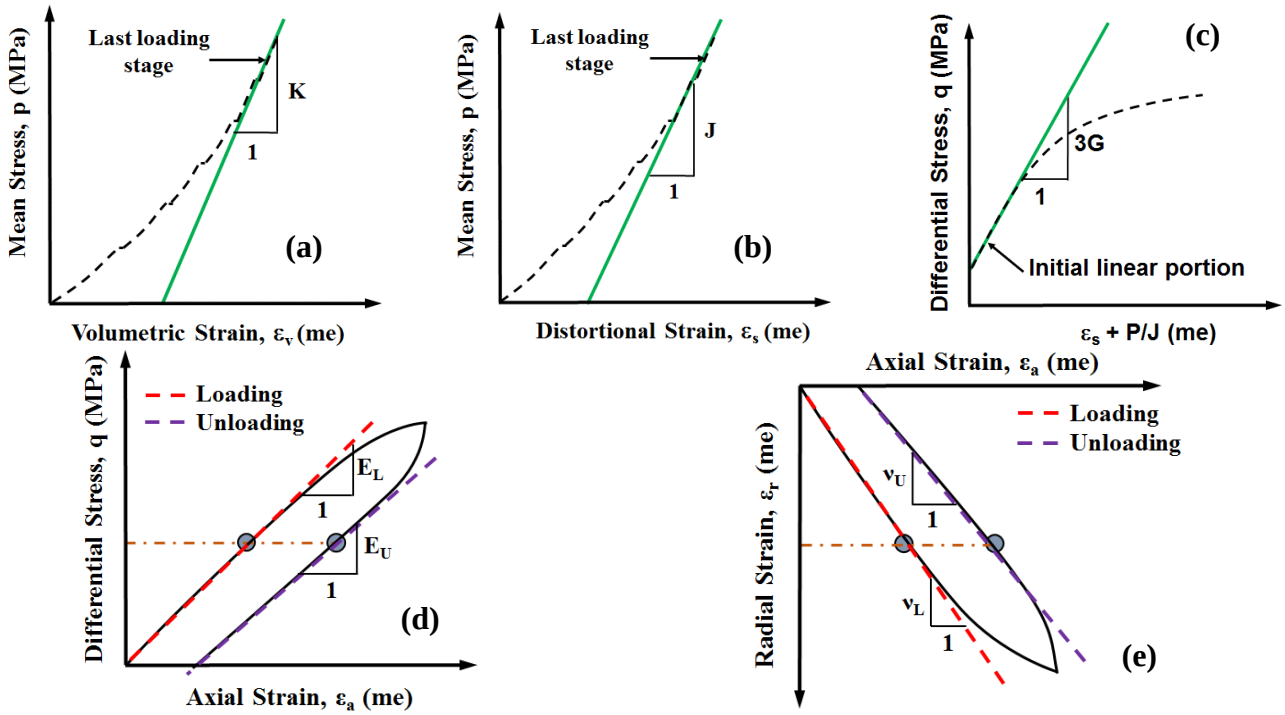

Fig. 2. Estimation of (a) bulk modulus (K), (b) coupling modulus (J), (c) shear modulus (G), (d) Young's modulus (E), and (e) Poisson's ratio (ν) using stress-strain data during the test (adapted and modified from Kamali-Asl et al., 2019).

2013; Villamor Lora et al., 2016; Kamali-Asl et al., 2019a). The stress path followed during an MSE test is shown in Fig. 3(a)-(e). Each level of CP was applied in an increment of 5 MPa and kept constant for 2 hours to ensure the full compaction (Fig. 3(a)). The MSE test was conducted under the CP of 0, 5, 10, 20, 30, 40, and 50 MPa, which are labeled as stages 1 through 7, respectively (Fig. (3a)). At the end of these CP stages, 1 to 4 cycles of DS were applied depending upon the CP level, as illustrated in Fig. 3(b)-(e). To stay within the elastic region, DS should not exceed 50% of UCS and 3 times of CP.

3.3.2. Cyclic Test

Reservoir rocks are subjected to cyclic loading due to various processes such as injection and extraction of fluids during operation and re-stimulation of fractures during permeability enhancement programs (e.g. Cha et al., 2017; Kamali-Asl et al., 2018b, 2019a). Therefore, cyclic tests are useful to characterize the gradual degradation of elasticity, non-linear and hysteresis behavior of rocks (e.g. Yang 2012; Kamali-Asl et al., 2018c, 2019a). As illustrated in Fig. 3(f), CP was gradually increased to 40 MPa, then 12 cycles of DS ranging from 5 to 60 MPa were applied to the specimen.

4. RESULTS AND DISCUSSION

4.1. Isotropic Compression

The isotropic compression test on the granodiorite specimen was performed by increasing the confining stress in a step-wise fashion from 0 to 50 MPa. For every increment of 5 MPa, CP was held constant for 15 minutes and then increased to the next level until it reached to a CP of 50 MPa. The bulk modulus is a good index for compressibility of the specimen under isotropic condition. As seen in Fig. 4(a), the bulk modulus of the specimen increased by increasing CP. This suggests the closure of the micro-cracks caused by stress relief during sampling process at all confining levels. However, the rate of increment in the bulk modulus is higher at lower confinement levels compared to that in higher confinement levels. This could be explained by the number of micro-cracks that remain open at different CP levels. For instance, most of the micro-cracks remain still open under lower CP, whereas only few micro-cracks remain open as CP is increased. Hence, lower potential increase in the compressibility (i.e. bulk modulus) at higher CP levels. The estimated coupling and shear moduli of the specimen are illustrated in Fig. 4(b) and (c). All of these moduli showed similar trend, i.e. higher rate of increment at lower confinement compare to higher confinement level. The pressure dependency of bulk, coupling, and shear moduli was observed in other studies (e.g. Sone and Zoback, 2013; Villamor Lora et al., 2016; Kamali-Asl et al., 2018b, 2019a).

4.2. MSE Test

Fig. 5(a)-(g) show the evolution of axial, radial, and volumetric strains against DS under different stages of the MSE test. Closure of the micro-cracks was observed at low initial DS levels (i.e. around 5 MPa), followed by a linear behavior for all stages of the test. In the case of zero

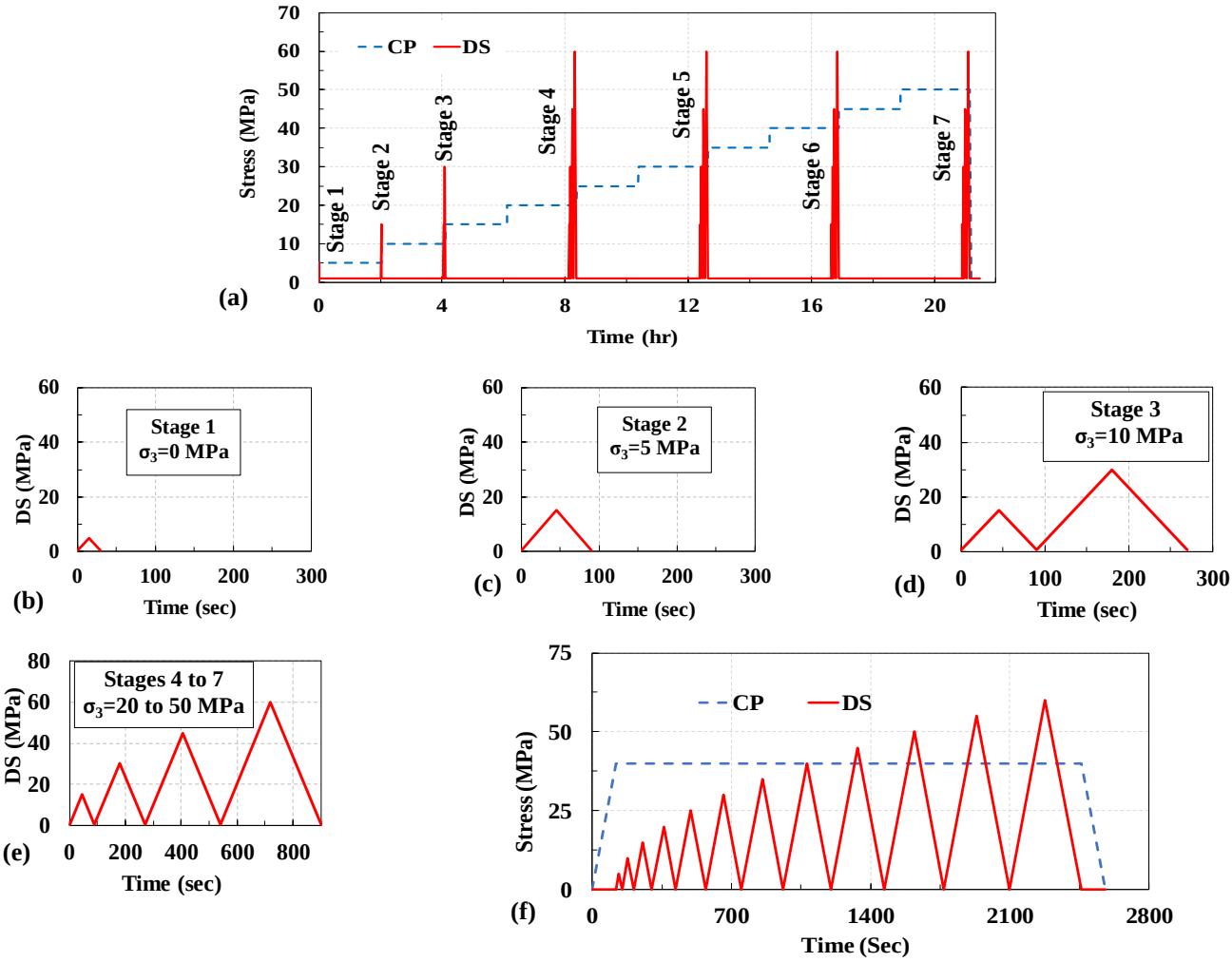

Fig. 3. (a) stress path followed during the MSE tests; differential stress during (b) Stage 1, (c) Stage 2, (d) Stage 3, and (e) Stages 4 to 7 of the test; and (f) stress path followed during the cyclic test.

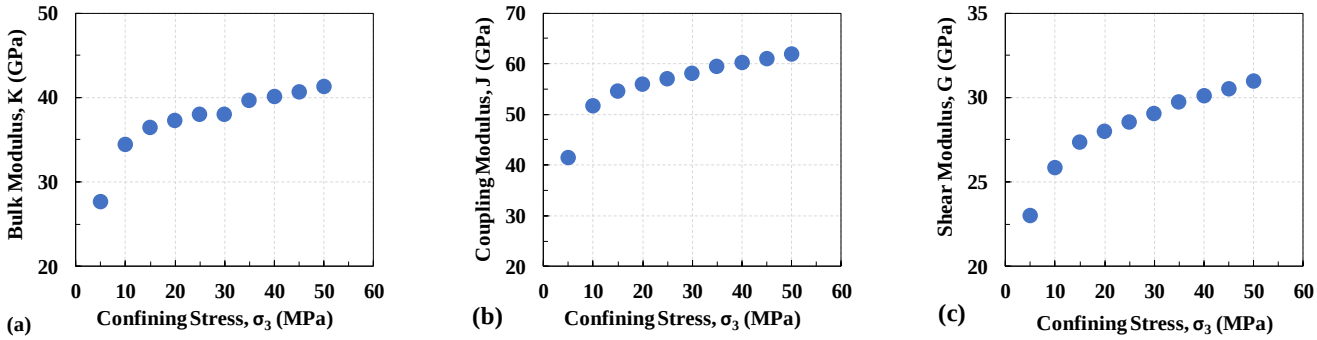

Fig. 4. Estimated static (a) bulk, (b) coupling, and (c) shear moduli at different confining levels

confinement (i.e. Stage 1; Fig 4(b)), applied DS was ~5 MPa. The stress-strain response of the specimen under such low (~5 MPa) DS level falls in the micro-crack closure region (see Fig 5(b) – (h)). The moduli measured under such DS level is not true elastic moduli of the specimen. Hence, elastic moduli during stage 1 of the MSE test (Fig 4(a) & (b)) are not reported in Table 1. The increase in the Young's modulus with the CP level under same axial loading is insignificant (Table 1), which indicates the pressure (confining) independency and linear behavior of the specimen under different CP levels tested in the study (e.g. Yang et al., 2015). However, higher Young's modulus was estimated under relatively higher DS levels at the same confinement. For instance, under all CPs during MSE test, Young's modulus increased with an increase in the DS level with more pronounced increment between DS of 30 and 45 MPa. This could be due to the presence of micro-cracks, which

did not completely close under all CPs and lower DS levels (i.e. up to 30 MPa). The higher Young's modulus during unloading stages, as observed in Table 1, is due to the fact that loading induces both elastic and plastic deformations in the specimen, which are not recovered during the unloading that is dominated by elastic deformations (e.g. Zoback, 2010; Sone and Zoback, 2013; Villamor Lora et al., 2016; Kamali-Asl et al., 2019a).

4.3. Cyclic Test

The evolution of axial, radial, and volumetric strains against DS in the cyclic test is shown in Fig. 5(h). Similar to MSE test results, Young's modulus and Poisson's ratio remained fairly similar under all the applied levels of DS (Table 2), which is also reflected in the linear behavior of the specimen illustrated in Fig. 5(h). The closure of the micro-cracks under lower DS levels was observed in the cyclic test as well. The insignificant difference between Young's modulus and Poisson's ratio during loading and unloading suggested very small plastic deformation, which is also reflected by negligible hysteresis behavior of the rock specimen (Fig 5(h)).

The elastic parameters of the granodiorite obtained in the study (Tables 1 and 2) are comparable with the previously published values for Aue granite i.e. 48 GPa at CP of 40 MPa (Hofmann et al. 2015), marble i.e. 58 GPa at CP of 35 MPa (Yang et al., 2015), Kuru granite i.e. 40 GPa at CP of 37.5 MPa (Hokka et al., 2016), and phyllite i.e. 55 GPa at CP of 40 MPa (Kamali-Asl et al., 2019a). Geomechanical and hydro-thermal responses of a deep geothermal reservoir are necessary in order to design the stimulation program for permeability enhancement (e.g. Majer et al., 2007), reduce the production decline over time, and build more accurate predictive models at reservoir scale (e.g. Ghassemi, 2012). Elastic moduli (i.e. Young's and shear moduli, and Poison's ratio) of the granodiorite specimen tested in the study indicated that the rock specimen has a high elasticity as compared to other typical geothermal reservoir rocks such as granite and sandstone (e.g. Ghassemi, 2012). High elasticity indicates the higher strength of the rock, which might affect the outcome of the hydraulic fracturing during reservoir stimulation of an EGS (e.g. Schön, 2015).

Thermal stresses induce thermal cracks in the reservoir rocks, which increase the reservoir permeability, but on the other hand, compromise the elastic and strength characteristics of the reservoir (e.g. Ghassemi, 2012). Although not investigated in this study, coupled thermal-hydrological-mechanical-chemical processes such as stress-corrosion, mechanical creep, pressure solution, free-face dissolution/precipitation of minerals (e.g. Ghassemi, 2012; Yasuhara et al., 2006; Kamali-Asl et al., 2019b) affects the productivity of the geothermal reservoir in a long run, which cannot be ruled out of the investigation.

Table 1. *E* and *ν* values during MSE test

CP (MPa)	DS (MPa)	*E* (GPa)		*ν*	
		L*	U*	L*	U*
0	0-5	NA	NA	NA	NA
5	0-15	71.92	71.00	0.24	0.25
10	0-15	69.94	72.17	0.24	0.25
	0-30	70.28	70.3	0.24	0.25
20	0-15	68.25	70.47	0.24	0.24
	0-30	69.32	71.13	0.24	0.25
	0-45	71.65	71.42	0.24	0.25
	0-60	71.07	70.57	0.24	0.24
30	0-15	68.64	71.22	0.24	0.24
	0-30	69.48	72.59	0.23	0.25
	0-45	71.09	72.36	0.24	0.24
	0-60	71.44	72.39	0.24	0.24
40	0-15	69.99	71.47	0.24	0.24
	0-30	69.79	72.48	0.23	0.24
	0-45	72.34	73.62	0.24	0.25
	0-60	73.03	73.17	0.24	0.24
50	0-15	71.73	72.50	0.24	0.25
	0-30	71.62	73.23	0.24	0.24
	0-45	73.67	73.62	0.24	0.25
	0-60	73.94	73.66	0.24	0.24

* L: Loading, U: Unloading, and NA: Not Applicable

Table 2. *E* and *ν* during cyclic test

DS (MPa)		E (GPa)		ν	
		L*	U*	L*	U*
CP = 40 MPa	0-5	93.20	94.11	0.25	0.25
	0-10	76.42	71.65	0.24	0.24
	0-15	73.08	71.05	0.25	0.25
	0-20	73.22	71.73	0.24	0.24
	0-25	72.75	71.82	0.24	0.24
	0-30	72.68	72.16	0.24	0.24
	0-35	73.11	72.54	0.24	0.24
	0-40	73.41	73.18	0.24	0.24
	0-45	73.63	73.33	0.24	0.24
	0-50	73.72	73.34	0.24	0.24
	0-55	73.79	73.54	0.24	0.24
	0-60	73.71	73.50	0.24	0.24

* L: Loading and U: Unloading

5. CONCLUSION

MSE and cyclic tests were conducted on an intact granodiorite specimen retrieved from Patua geothermal field. MSE test was performed at seven different confining levels ranging from 0 to 50 MPa, while the cyclic test was performed under the confining level of 40 MPa (i.e. in-situ overburden stress) and differential stress ranging from 5 to 60 MPa. Static moduli of the specimen were estimated from the stress-strain response of the specimen during the tests. During isotropic compression, static bulk modulus increased at higher rate under lower CP compared to that at higher CP. Most of the micro-cracks present in the rock closes at the lower CP values, and hence, the higher rate of increment of bulk modulus at lower CP values. The Young's modulus of the

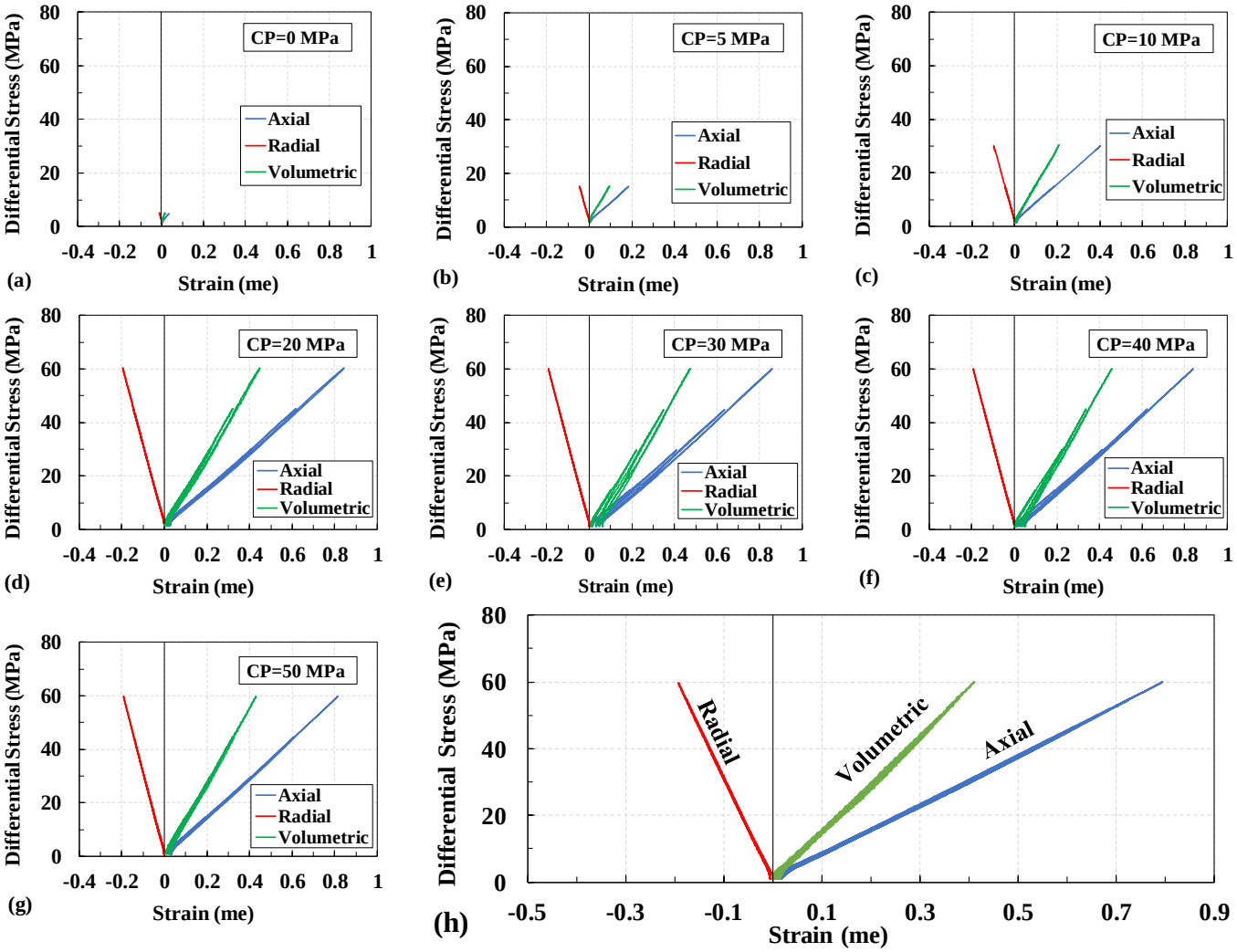

Fig. 5. Evolution of axial, radial, and volumetric strain at CP levels of (a) 0, (b) 5, (c) 10, (d) 20, (e) 30, (f) 40, (g) 50 MPa during the MSE test, and (h) cyclic test

specimen showed a pronounced increment between 30 and 45 MPa, which could be due to the presence of micro-cracks that close at higher DS levels. Moreover, Young's modulus during the unloading path was higher compared to that of loading path because of the fact that both elastic and plastic deformations occur during loading whereas only elastic deformations are recovered during unloading. The plastic deformations during the tests were insignificant, which explain the linear response with negligible hysteresis behavior of the specimen. The results obtained in the study agree with the previously-published results. The laboratory mechanical characterization of a rock specimen is a short term test and does not account for a long term chemical changes in the rock specimens in the in situ conditions. Therefore, it should be acknowledged that the material properties of the reservoir rocks might change over the time. Other tests such as creep, multi-stage failure tests, and flow-through tests to characterize the viscoelastic response, strength properties, and flow properties of the specimen are in progress.

6. ACKNOWLEDGEMENT

The authors would like to thank AltaRock Energy Inc. and University of Nevada, Reno for providing the rock core used in this study. We would also like to thank Mr. Marco vanGemeren at Mineral Optics Laboratory for preparing the specimens, and Professor Nico Perdrial at University of Vermont for his constructive feedback and help with XRD analysis.

7. REFERENCES

1. ASTM D4543-08, "Standard Practices for Preparing Rock Core as Cylindrical Test Specimens and Verifying Conformance to Dimensional and Shape Tolerances." ASTM International, West Conshohocken, PA, 2008, DOI: 10.1520/D4543-08

2. ASTM D7012, "Standard Test Methods for Compressive Strength and Elastic Moduli of Intact Rock Core Specimens under Varying States of Stress and Temperatures." Philadelphia: ASTM.

3. Cha, M., Alqahtani, N. B., Yin, X., Kneafsey, T. J., Yao, B., & Wu, Y. S. (2017). Laboratory system for studying cryogenic thermal rock fracturing for well stimulation. Journal of Petroleum Science and Engineering, 156, 780-789.

4. Cladouhos, T.T., Petty, S., Swyer, M.W., Uddenberg, M.E., Grasso, K., Nordin, Y., (2016). Results from newberry volcano EGS demonstration, 2010–2014. Geothermics, 63, 44–61.

5. Combs, J., Peterson, N., Garg, S. K., & Goranson, C. (2012). "Reservoir testing and analysis at the Patua geothermal federal unit, Northwestern Nevada." GRC Trans, 36, 31-6.

6. Garg, S. K., Goranson, C., Johnson, S., & Casteel, J. (2015). Reservoir Testing and Modeling of the Patua Geothermal Field, Nevada, USA. Proc., WGC.

7. Ghassemi, A. (2012). A review of some rock mechanics issues in geothermal reservoir development. Geotechnical and Geological Engineering, 30(3), 647-664.

8. Glazner, A. F., Bartley, J. M., Coleman, D. S., Cawood, A. J., & Bond, C. E. (2019). A More Informative Way to Name Plutonic Rocks. GSA Today, 29(2).

9. Guo, L. L., Zhang, Y. B., Zhang, Y. J., Yu, Z. W., & Zhang, J. N. (2018). "Experimental investigation of granite properties under different temperatures and pressures and numerical analysis of damage effect in enhanced geothermal system." Renewable energy, 126, 107-125.

10. Hofmann, H., Babadagli, T., Yoon, J. S., Zang, A., & Zimmermann, G. (2015). A grain based modeling study of mineralogical factors affecting strength, elastic behavior and micro fracture development during compression tests in granites. Engineering Fracture Mechanics, 147, 261-275.

11. Hokka, M., Black, J., Tkalich, D., Fourmeau, M., Kane, A., Hoang, N. H., ... & Kuokkala, V. T. (2016). Effects of strain rate and confining pressure on the compressive behavior of Kuru granite. International Journal of Impact Engineering, 91, 183-193.

12. Islam, M. A., & Skalle, P. (2013). An experimental investigation of shale mechanical properties through drained and undrained test mechanisms. Rock Mechanics and Rock Engineering, 46(6), 1391-1413.

13. Kamali-Asl, A., Ghazanfari, E., Hedayat, A., & Deering, L. (2018b). "Investigation of static/dynamic moduli and plastic response of shale specimens." International Journal of Rock Mechanics and Mining Sciences, 110, 231-245.

14. Kamali-Asl, A., Ghazanfari, E., Newell, P., & Stevens, M. (2018c). Elastic, viscoelastic, and strength properties of Marcellus Shale specimens. Journal of Petroleum Science and Engineering, 171, 662-679.

15. Kamali-Asl, A., Ghazanfari, E., Perdrial, N., & Bredice, N. (2018a). Experimental study of fracture response in granite specimens subjected to hydrothermal conditions relevant for enhanced geothermal systems. *Geothermics*, *72*, 205-224.

16. Kamali-Asl, A., Kc, B., Foroutan, M., Ghazanfari, E., Cladouhos, T. T., & Stevens, M. (2019a). "Stress-strain response and seismic signature analysis of phyllite reservoir rocks from Blue Mountain geothermal field." *Geothermics*, *77*, 204-223.

17. Kamali-Asl, A., KC, B., Ghazanfari, E., & Hedayat, A. (2019b). Flow-induced alterations of ultrasonic signatures and fracture aperture under constant state-of-stress in a single-fractured rock. Geophysics, 84(4), 1-58.

18. Kumar, A. A., Reddy, T. G., David, J. S., Randive, K. R., Tripathy, A. K., & Murthy, P. R. (2017). Petro-mineralogical characterization of the compositionally expanded Tonalite-Granodiorite-Monzogranite (TGM) suite of granitoids showing evidences of magma mixing and mingling in parts of Eastern Dharwar Craton, India.

19. Kwon, S., Xie, L., Park, S., Kim, K. I., Min, K. B., Kim, K. Y., Zhuang, L., Choi, J., Kim, H., & Lee, T. J. (2018). Characterization of 4.2-km-Deep Fractured Granodiorite Cores from Pohang Geothermal Reservoir, Korea. *Rock Mechanics and Rock Engineering*, 1-12.

20. Li, X. B., Lok, T. S., & Zhao, J. (2005). Dynamic characteristics of granite subjected to intermediate loading rate. Rock Mechanics and Rock Engineering, 38(1), 21-39.

21. Lutz, S. J., Hickman, S., Davatzes, N., Zemach, E., Drakos, P., & Robertson-Tait, A. (2010, February). Rock mechanical testing and petrologic analysis in support of well stimulation activities at the Desert Peak Geothermal Field, Nevada. In *Proceedings 35th workshop on geothermal reservoir engineering*.

22. Majer, E. L., Baria, R., Stark, M., Oates, S., Bommer, J., Smith, B., & Asanuma, H. (2007). Induced seismicity associated with enhanced geothermal systems. Geothermics, 36(3), 185-222.

23. McClure, M. W., & Horne, R. N. (2014). An investigation of stimulation mechanisms in Enhanced Geothermal Systems. *International Journal of Rock Mechanics and Mining Sciences*, *72*, 242-260.

24. Motra, H. B., & Stutz, H. H. (2018). "Geomechanical Rock Properties Using Pressure and Temperature Dependence of Elastic P-and S-Wave Velocities." *Geotechnical and Geological Engineering*, *36*(6), 3751-3766.

25. Nejati, M. (2018). On the anisotropy of mechanical properties in Grimsel granodiorite. ETH Zurich.

26. Oldenburg, C. M., Dobson, P. F., Wu, Y., Cook, P. J., Kneafsey, T. J., Nakagawa, S., ... & Rutqvist, J. (2017, February). Hydraulic fracturing experiments at 1500 m depth in a deep mine: Highlights from the kISMET project. *In Proceedings, 42nd Workshop on Geothermal Reservoir Engineering, Stanford University*.

27. Pellegrino, A., Sulem, J., & Barla, G. (1997). The effects of slenderness and lubrication on the uniaxial

behavior of a soft limestone. International Journal of Rock Mechanics and Mining Sciences, 34(2), 333-340.

28. Peterson, N., Combs, J., Bjelm, L., Garg, S., Kohl, B., Goranson, C., Merrill, R., Kamp, V. D. P & Lamb¹, A. (2011). Integrated 3D Modeling of Structural Controls and Permeability Distribution in the Patua Geothermal Field, Hazen, NV. *Bulletin, V, 95*(7), 1147-1180.

29. Pour, A. B., Hashim, M., Park, Y., & Hong, J. K. (2018). Mapping alteration mineral zones and lithological units in Antarctic regions using spectral bands of ASTER remote sensing data. *Geocarto International*, *33*(12), 1281-1306.

30. Puzrin AM (2012) Constitutive modelling in geomechanics. Springer, Berlin. doi: 10.1007/978-3-642-27395-7

31. Riahi, A., & Damjanac, B. (2013, February). Numerical study of hydro-shearing in geothermal reservoirs with a pre-existing discrete fracture network. In *Proceedings of the 38th Workshop on Geothermal Reservoir Engineering, Stanford, CA* (pp. 11-13).

32. Sarjoughian, F., & Kananian, A. (2017). Zircon U-Pb geochronology and emplacement history of intrusive rocks in the Ardestan section, central Iran. *Geologica acta*, *15*(1), 0025-36.

33. Schön, J. H. (2015). Physical properties of rocks: Fundamentals and principles of petrophysics (Vol. 65). Elsevier.

34. Sone, H., & Zoback, M. D. (2013). "Mechanical properties of shale-gas reservoir rocks—Part 1: Static and dynamic elastic properties and anisotropy." *Geophysics*, 78(5), D381-D392.

35. Tester, J. W., Anderson, B. J., Batchelor, A. S., Blackwell, D. D., DiPippo, R., Drake, E., ... & Petty, S. (2006). The future of geothermal energy: Impact of enhanced geothermal systems (EGS) on the United States in the 21st century. *Massachusetts Institute of Technology*, *209*.

36. Villamor Lora, R., Ghazanfari, E., & Izquierdo, E. A. (2016). "Geomechanical characterization of Marcellus shale." *Rock Mechanics and Rock Engineering*, 49(9), 3403-3424

37. Wang, S., Li, X., Du, K., Wang, S., & Tao, M. (2018). Experimental study of the triaxial strength properties of hollow cylindrical granite specimens under coupled external and internal confining stresses. Rock Mechanics and Rock Engineering, 51(7), 2015-2031.

38. Watanabe, N., Egawa, M., Sakaguchi, K., Ishibashi, T., & Tsuchiya, N. (2017). Hydraulic fracturing and permeability enhancement in granite from subcritical/brittle to supercritical/ductile conditions. *Geophysical Research Letters*, *44*(11), 5468-5475.

39. White, M., Fu, P., McClure, M., Danko, G., Elsworth, D., Sonnenthal, E., Kelkar, S., & Podgorney, R. (2018). A suite of benchmark and challenge problems for enhanced geothermal systems. *Geomechanics and Geophysics for Geo-Energy and Geo-Resources*, *4*(1), 79-117.

40. Wiener, J. M., Ramurthy, M., Kundert, D. P., Le Tran, J. B., & Stephens, M. R. (2019). *U.S. Patent Application No. 15/983,570.*

41. Yan, X., Jun, L., Gonghui, L., & Xueli, G. (2017). Mechanical Properties and Acoustic Emission Properties of Rocks with Different Transverse Scales. Shock and Vibration, 2017.

42. Yang, S. Q. (2012). Strength and deformation behavior of red sandstone under multi-stage triaxial compression. Canadian Geotechnical Journal, 49(6), 694-709.

43. Yang, S. Q., Xu, P., Ranjith, P. G., Chen, G. F., & Jing, H. W. (2015). Evaluation of creep mechanical behavior of deep-buried marble under triaxial cyclic loading. Arabian Journal of Geosciences, 8(9), 6567-6582.

44. Yasuhara, H., Polak, A., Mitani, Y., Grader, A. S., Halleck, P. M., & Elsworth, D. (2006). Evolution of fracture permeability through fluid–rock reaction under hydrothermal conditions. Earth and Planetary Science Letters, 244(1-2), 186-200.

45. Zhang, Y., Hao, S., Bai, L., Yu, Z., Zhang, J., & Fang, J. (2018). Thermomechanical Behavior of Late Indo-Chinese Granodiorite under High Temperature and Pressure. *Journal of Engineering*, *2018.*

46. Zoback, M. D. (2010). "Reservoir Geomechanics." Cambridge University Press.